catalysts

MDPI

Article

Effect of Different Zinc Species on Mn-Ce/CuX Catalyst for Low-Temperature NH_3-SCR Reaction: Comparison of $ZnCl_2$, $Zn(NO_3)_2$, $ZnSO_4$ and $ZnCO_3$

Lin Chen [1,2], Shan Ren [1,*], Tao Chen [1], Xiaodi Li [1], Zhichao Chen [1], Mingming Wang [1], Qingcai Liu [1] and Jie Yang [3,*]

[1] College of Materials Science and Engineering, Chongqing University, Chongqing 400044, China; lin.chen@cqu.edu.cn (L.C.); 202209131182@stu.cqu.edu.cn (T.C.); lxd199611@126.com (X.L.); 20162749@cqu.edu.cn (Z.C.); 202009131184@cqu.edu.cn (M.W.); liu_qingcai@163.com (Q.L.)
[2] Bioenergy and Catalysis Laboratory, Paul Scherrer Institute (PSI), CH-5232 Villigen, Switzerland
[3] College of Chemistry and Chemical Engineering, Wuhan Textile University, Wuhan 430200, China
* Correspondence: shan.ren@cqu.edu.cn (S.R.); yangjie@wtu.edu.cn (J.Y.)

Abstract: The effects of four distinct zinc species ($ZnCl_2$, $Zn(NO_3)_2$, $ZnSO_4$, and $ZnCO_3$) on a Mn-Ce co-doped CuX (MCCX)catalyst were investigated and contrasted in the low-temperature NH_3-SCR process. Aqueous solutions of $ZnCl_2$, $Zn(NO_3)_2$, $ZnSO_4$, and $ZnCO_3$ were used to poison the catalysts. The catalytic activity of all catalysts was assessed, and their physicochemical properties were studied. There was a notable drop trend in catalytic activity in the low temperature range (200 °C) after zinc species poisoning on MCCX catalyst. Interestingly, $ZnSO_4$ and $ZnCO_3$ on MCCX catalyst had more serious effect on catalytic activity than $Zn(NO_3)_2$ and $ZnCl_2$ from 150 °C to 225 °C, in which NO conversion of the MCCX-Zn-S and MCCX-Zn-C catalysts dropped about 20–30% below 200 °C compared with the fresh MCCX catalyst. The zeolite X structure was impacted by Zn species doping on the MCCX catalyst, and the Zn-poisoned catalysts had less acidic and lower redox ability than fresh Mn-Ce/CuX catalysts. Through the results of in situ DRIFTS spectroscopy experiments, all catalysts were governed by both Langmuir–Hinshelwood (L–H) and Eley–Rideal (E–R) mechanisms, and the possible mechanism for poisoning the Mn-Ce/CuX catalyst using various zinc species was revealed.

Keywords: Mn-Ce/CuX catalyst; zinc species poisoning; low-temperature NH_3-SCR

Citation: Chen, L.; Ren, S.; Chen, T.; Li, X.; Chen, Z.; Wang, M.; Liu, Q.; Yang, J. Effect of Different Zinc Species on Mn-Ce/CuX Catalyst for Low-Temperature NH_3-SCR Reaction: Comparison of $ZnCl_2$, $Zn(NO_3)_2$, $ZnSO_4$ and $ZnCO_3$. *Catalysts* **2023**, *13*, 1219. https://doi.org/10.3390/catal13081219

Academic Editors: Yun Zheng and De Fang

Received: 13 July 2023
Revised: 10 August 2023
Accepted: 11 August 2023
Published: 17 August 2023

1. Introduction

The worldwide deterioration in air quality has led to the establishment of stronger rules on the emission of nitrogen oxides (NO_x) [1,2]. The selective catalytic reduction (SCR) of NO_x with NH_3 is a well-established and widely utilized technology [3]. According to a number of studies [4–6], despite its popularity, the commercial V_2O_5-$WO_3(MoO_3)/TiO_2$ catalyst has a few limitations that prevent it from being truly helpful. It is hazardous to living things because of vanadium species, does not work well at lower temperature, and can only be used effectively between 350 and 450 °C. This shows how important it is to look into low-temperature SCR catalysts that do not use vanadium to control NO_x emissions.

Compared to vanadium-based catalysts, copper-based catalysts have better redox properties and thermodynamic stabilities [7,8], making them a viable alternative. It was discovered by Wang et al. [9] that the maximum NO conversion of the Cu-ZSM-5 catalyst occurred between 200 and 400 °C, with practically full conversion, because of the highly preferential production of active copper species and the quick flip between Cu^{2+} and Cu^{+} species during the NH_3-SCR process. Cu-exchanged zeolite catalysts have recently been the subject of extensive study in NH_3-SCR reaction [10,11]. Tarach et al. [12] compared the activity and stability of Cu-exchanged zeolites with different framework topologies in NH_3-SCR reaction and found that the Cu-ZSM-5 catalyst displayed an extraordinary activity in the NH_3-SCR process, achieving nearly 100% NO conversion at 175 °C with almost

100% N_2 selectivity. Our prior research [13,14] found that zeolite X could be generated cheaply from the blast furnace slag, making ion-exchange techniques a viable option for producing CuX zeolite catalyst. Doping Mn and Ce oxides on CuX zeolite could improve its SO_2 + H_2O resistance and enhance its low-temperature NH_3-SCR activity. Generally, the catalysts nevertheless often experienced severe poisoning by alkali, alkaline earth, and heavy metals in the actual fuel gas state. The deactivation rate of various poisonous zinc species was shown to be in the order of $ZnCl_2$ > $ZnSO_4$ > ZnO by Wang et al. [15], who studied the effects of three distinct zinc species (ZnO, $ZnSO_4$, and $ZnCl_2$) on Sb-$CeZr_2O_x$ catalysts. According to our earlier research [16,17], $ZnCl_2$ had a more severe poisoning effect on the Mn-Ce/AC catalyst than $ZnSO_4$, and Zn^{2+} would occupy the acidic site of the catalyst after loading zinc salts. Nonetheless, the poisoning impact of various zinc species on Cu-exchanged zeolite catalysts has received insufficient attention till now.

The current research looked into how different zinc ions affected the catalytic performance of the Mn-Ce/CuX catalyst in low-temperature denitration reactions. To poison the Mn-Ce/CuX catalyst, we used an impregnation technique with $ZnCl_2$, $Zn(NO_3)_2$, $ZnSO_4$, and $ZnCO_3$ solutions. The causes of zinc salt poisoning and deactivation of the Mn-Ce/CuX catalyst have been identified, and the possible mechanism for poisoning the Mn-Ce/CuX catalyst using various zinc salts has been proposed, by comparing the catalytic activity, dispersion degree of active component, surface morphology and pore structure, surface acidity, redox performance, element concentration of active component, and surface reaction path of the catalyst before and after poisoning.

2. Results and Discussions

2.1. Denitration Performance

The catalytic activity for fresh MCCX and catalysts poisoned with different Zn species (MCCX-Zn-Cl, MCCX-Zn-N, MCCX-Zn-S, and MCCX-Zn-C catalysts) can be found in Figure 1. NO conversion of Zn-poisoned catalysts is much lower than that of the fresh MCCX catalyst at temperatures below 200 °C, as seen in Figure 1a. In detail, NO conversion of the MCCX-Zn-C catalyst surpassed the other three poisoned catalysts at temperatures below 125 °C, whereas NO conversion of the MCCX-Zn-Cl catalyst outperformed the other three Zn-poisoned catalysts at temperatures over 150 °C, reaching nearly 100% at 275 °C. The NO conversion rate for the MCCX-Zn-S and MCCX-Zn-C catalysts dropped by about 20–30% below 200 °C, making it the worst performing catalyst over the whole reaction temperature range. It was discovered that the conversion of the catalysts is most affected by the different Zn species in the lower temperature range, whereas they have almost no effect at higher temperatures. According to Figure 1b, comparing the N_2 selectivity of the MCCX-Zn-Cl, MCCX-Zn-N, MCCX-Zn-S, and MCCX-Zn-C catalysts to that of the fresh MCCX catalyst, there was an approximate 20% improvement. Figure 1c displays the results of a measurement of the concentration of NH_3 and N_2O in both Zn-poisoned and new MCCX catalysts. Zn-poisoned catalysts had lower concentrations of N_2O and higher concentrations of NH_3 compared to the fresh MCCX catalyst, among which the MCCX-Zn-S sample also had more NH_3 than N_2O.

2.2. Structural Properties

X-ray diffraction (XRD) patterns of MCCX, MCCX-Zn-Cl, MCCX-Zn-N, MCCX-Zn-S, and MCCX-Zn-C catalysts are shown in Figure 2. The zeolite X structure was described by peaks at 2theta = 6.8°, 15.5°, 18.5°, 20.2°, 23.4°, 26.8°, and 30.5°, while the CuO phases were characterized by peaks at 2theta = 35.5°, 38.9°, 48.8°, and 61.5°. It was discovered that the peak intensity of zeolite X on Zn-poisoned catalysts was lesser than on the fresh catalyst, whereas the peak intensity of CuO phase on Zn-poisoned catalysts was stronger than on the fresh one. It was noted that the peak intensity of zeolite X on the MCCX-Zn-Cl catalyst was much stronger than the other three catalysts, while the peak intensity of zeolite X on MCCX-Zn-S and MCCX-Zn-C catalysts were weaker. This result suggested that the zeolite X structure was impacted by Zn species doping on MCCX catalyst, and the zinc species

contributed to the migration of CuO species. The absence of the Zn species peak indicates that they are uniformly dispersed on the catalyst surface. Micrographs of the catalysts (Figure 3) show that Zn-poisoned catalysts had a zeolite X structure that deviated from the usual octahedron, and some of the zeolite X particles agglomerated. In particular, the zeolite X structure of the MCCX-Zn-C catalyst had more serious damage than the other three catalysts. Furthermore, EDS mapping revealed that Cu aggregated on catalysts due to Zn poisoning, leading to an insufficiency of Cu active sites.

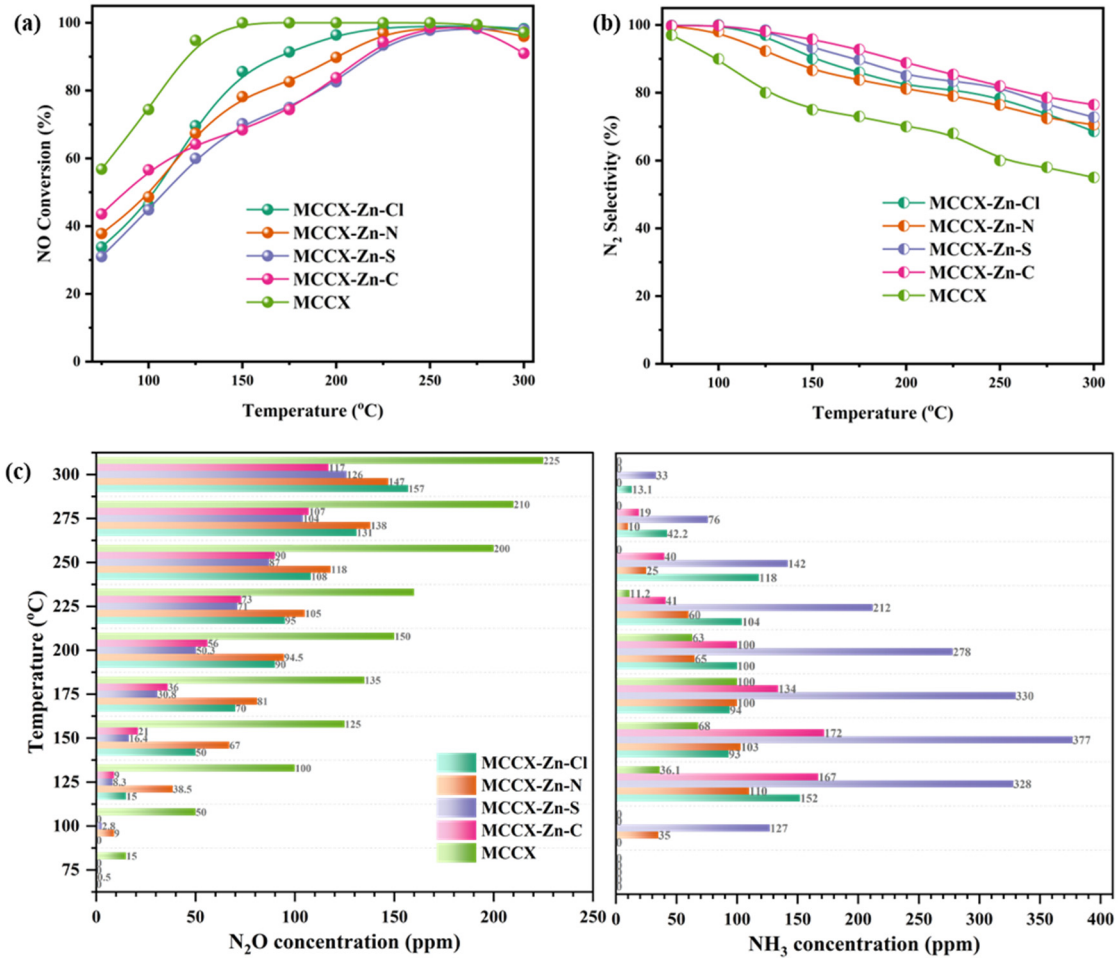

Figure 1. NH_3-SCR performance with temperature for MCCX, MCCX-Zn-Cl, MCCX-Zn-N, MCCX-Zn-S, and MCCX-Zn-C catalysts: (**a**) NO conversion; (**b**) N_2 selectivity; (**c**) N_2O and NH_3 concentration. Reaction conditions: 500 ppm NO, 500 ppm NH_3, 11% O_2, N_2 as balance, and GHSV of 36,000 h^{-1}.

2.3. XPS Analysis

To find out more about the elemental compositions of the MCCX-Zn-Cl, MCCX-Zn-N, MCCX-Zn-S, and MCCX-Zn-C catalysts, XPS spectra of Cu 2p, O 1s, Mn 2p, and Zn 2p were measured, as displayed in Figure 4. Peaks at the 948–966 eV, 940–945 eV, and 930–948 eV regions in the Cu 2p spectra (Figure 4a) were attributed to Cu $2p_{1/2}$, satellite peaks, and Cu $2p_{3/2}$, respectively [11,12]. Additionally, the spectra of Cu $2p_{3/2}$ could be divided into two peaks; one at 935 eV was attributed to Cu^{2+}, and another at 933 eV was attributed to Cu^{+} ions [9,10,18,19]. By calculating the area of the corresponding peaks, we were able to determine the relative abundance of the different Cu species and establish the following ranking for the concentration of Cu^{2+} species: the MCCX-Zn-S catalyst (45.1%) was more effective than the MCCX-Zn-N catalyst (43.5%), MCCX-Zn-Cl catalyst (39.7%), and MCCX-Zn-C catalyst (37.1%). In general, the isolated state of Cu^{2+} species in the zeolite lattice was an active site during the catalytic process [8,20,21].

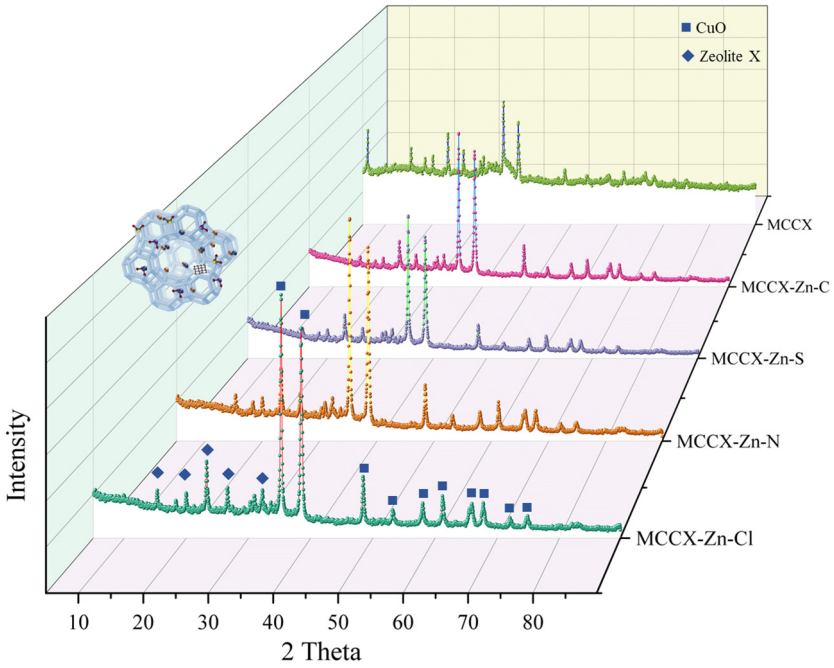

Figure 2. XRD patterns of MCCX, MCCX-Zn-Cl, MCCX-Zn-N, MCCX-Zn-S, and MCCX-Zn-C catalysts.

Figure 4b shows the XPS spectra of Mn 2p for MCCX-Zn-Cl, MCCX-Zn-N, MCCX-Zn-S, and MCCX-Zn-C catalysts. Mn $2p_{3/2}$ and Mn $2p_{1/2}$ were responsible for the two large peaks seen at about 642 and 650 eV, respectively [22]. In addition, three fitting peaks at about 641.5 eV, 640.5 eV, and 639.2 eV were identified in the spectra of Mn $2p_{3/2}$, which corresponded to Mn^{4+}, Mn^{3+}, and Mn^{2+} species, respectively [23–25]. The concentration order of species Mn4+ was as follows: MCCX-Zn-N > (32.5%) > MCCX-Zn-Cl (30.7%) > MCCX-Zn-C (26.8%) > MCCX-Zn-S (22.5%) catalysts. Previous studies indicated that high valve state Mn species (Mn^{4+} species) facilitated NO oxidation to NO_2 and accelerated the "fast SCR" process at low temperatures [26,27].

O 1s spectra of MCCX-Zn-Cl, MCCX-Zn-N, MCCX-Zn-S, and MCCX-Zn-C catalysts were depicted in Figure 4c. Three fitting peaks at around 531.6 eV, 529.5 eV, and 533.5 eV belonged to chemosorbed oxygen species (O_α), lattice oxygen species (O_β), and chemisorbed oxygen or weakly bound oxygen species (O_γ), respectively [28–30]. Generally, the catalysts exhibited the increased NH_3-SCR activity at higher concentrations of chemosorbed oxygen species due to their greater mobility in comparison to the other two oxygen species [13,23,31]. The concentration order of species O_α was as follows: MCCX-Zn-S (66.7%) > MCCX-Zn-C (57.1%) > MCCX-Zn-Cl (55.8%) > MCCX-Zn-N (50.5%) catalysts. The SO_4^{2-} and CO_3^{2-} might provide more chemosorbed oxygen species on catalysts, which was in line with the previous study [32]. In Figure 4d, there is one peak belonging to Zn $2p_{3/2}$ that could be found at Zn-poisoned catalysts [33]. The weakest peak intensity of the four catalysts was observed in the MCCX-Zn-S catalyst from the summary XPS spectra displayed in Figure 4e, attesting to the low amount of the surface's active components and, consequently, lesser SCR activity.

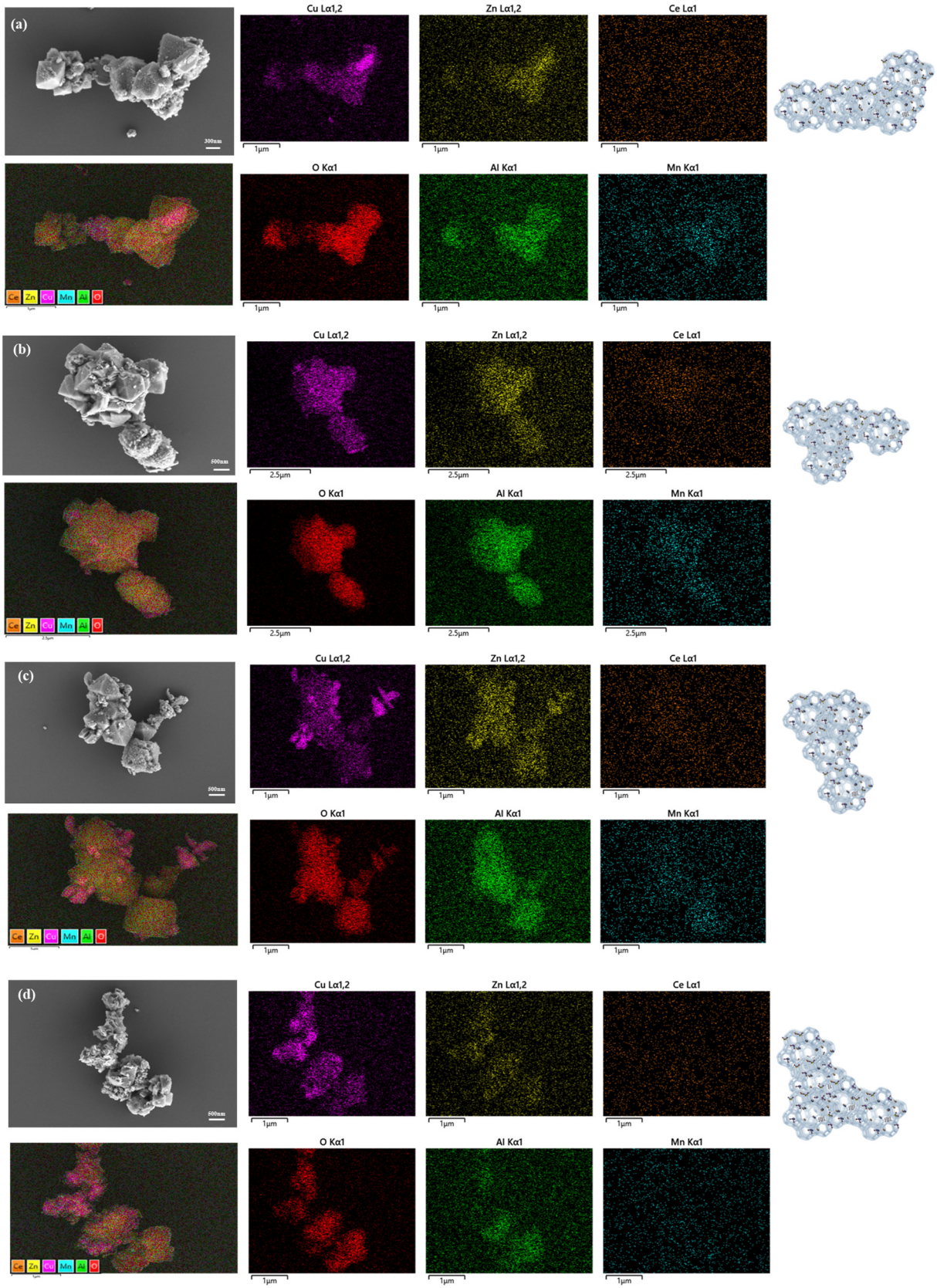

Figure 3. SEM images and elements mapping of (**a**) MCCX-Zn-Cl, (**b**) MCCX-Zn-N, (**c**) MCCX-Zn-S, and (**d**) MCCX-Zn-C catalysts.

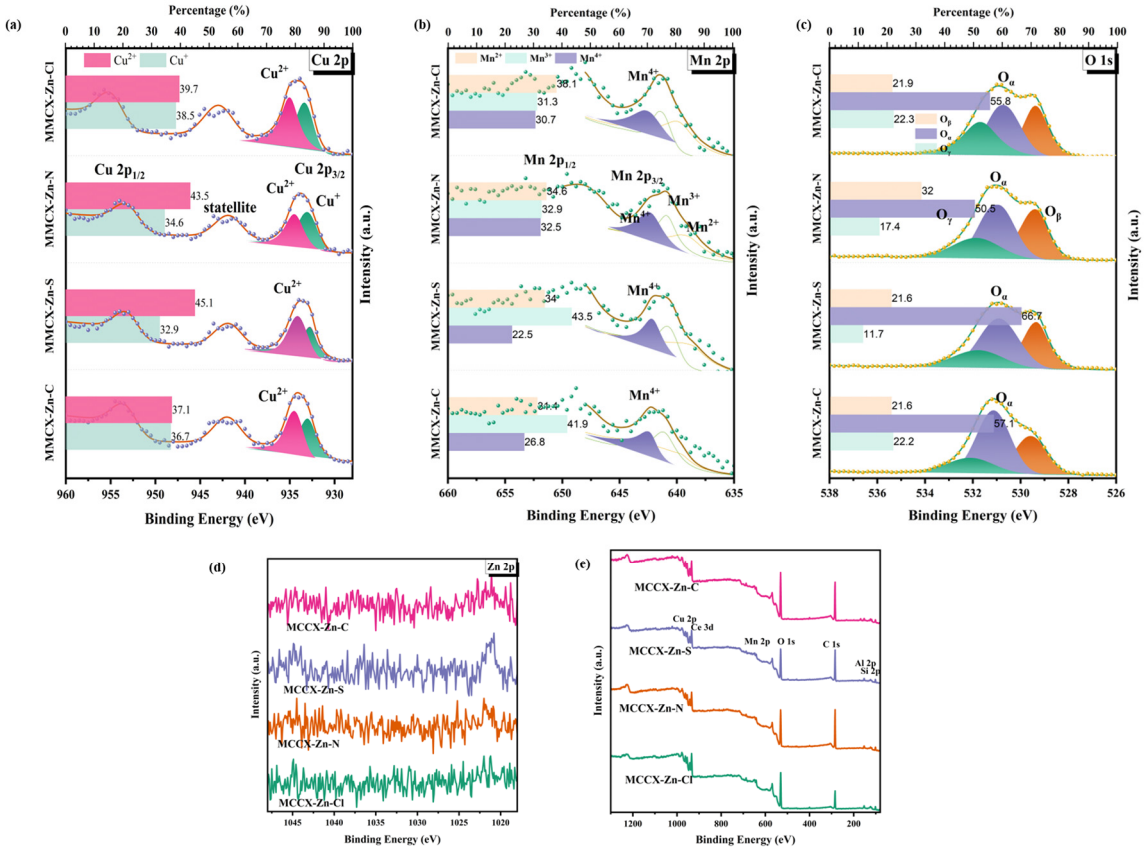

Figure 4. XPS spectra of MCCX-Zn-Cl, MCCX-Zn-N, MCCX-Zn-S, and MCCX-Zn-C catalysts: (**a**) Cu 2p (purple solid dots were assigned to the original data, red line was assigned to the fitting curve); (**b**) Mn 2p (green solid dots were assigned to the original data, deep yellow line was assigned to the fitting curve); (**c**) O 1 s (golden yellow solid dots were assigned to the original data, green line was assigned to the fitting curve); (**d**) Zn 2p; and (**e**) survey spectrum.

2.4. Acidity and Redox Property

The main factor in SCR activity is the acidity of the catalyst's surface. Figure 5a–c shows the NH_3-TPD results and in situ DRIFTS spectra of NH_3 desorption at temperatures between 35 and 300 °C for MCCX-Zn-Cl, MCCX-Zn-N, MCCX-Zn-S, and MCCX-Zn-C catalysts. Figure 5a shows that all Zn-poisoned catalysts exhibit several fitting peaks between 100 and 800 °C. The peak at 122 °C is associated with low acidity, those between ca. 200 and 400 °C are linked to medium acidity, and those beyond 400 °C are associated with high acidity [14,32,34]. In addition, as shown in Figure 5b, the area of fitting peaks was used to determine the amount of adsorbed NH_3. All the catalysts were found to have a greater middle acidity, and the following list shows what they ranked in terms of how much NH_3 they were able to absorb: concentrations of MCCX-Zn-Cl (478.1 μmoL/g), MCCX-Zn-C (435.9 μmoL/g), MCCX-Zn-N (299.1 μmoL/g), and MCCX-Zn-S (219.8 μmoL/g). Figure 5c shows the in situ DRIFTS spectra of NH_3 desorption, which shows multiple bands on each of the four catalysts between 3000 and 3800 cm^{-1}. These bands were assigned to Cu^{2+} absorbed NH_3 species (3182 and 3332 cm^{-1}) and NH_4^+ species on Brønsted acid sites (3272 cm^{-1}) [9,35]. Bands corresponding to coordinated adsorbed NH_3 species on Lewis acid sites (1610 and 1260 cm^{-1}) and NH_4^+ species on Brønsted acid sites (1390 cm^{-1}) were also observed [36,37]. The acidity reduced as the reaction temperature increased, which can be seen from the gradual dropping in peak intensity of the acid sites. Lewis acid sites on catalysts were also shown to be more stable than Brønsted acid sites, indicating that Lewis acid sites were the most important acid sites for the reactions.

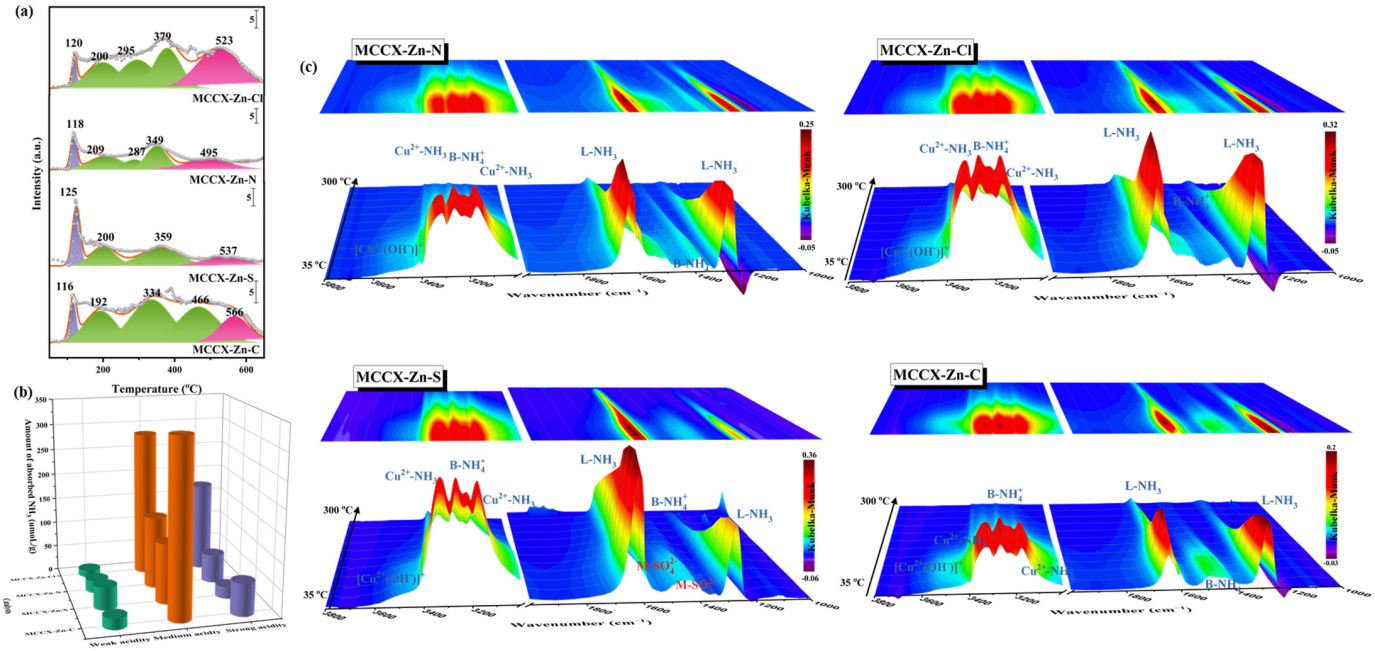

Figure 5. (**a**) NH_3-TPD profiles of all catalysts (purple fitting peaks belonged to weak acidity, green fitting peaks belonged to medium acidity and pink fitting peak belonged to strong acidity) and (**b**) integral area of peaks from NH_3-TPD profiles; (**c**) in situ DRIFTS spectra of NH_3 adsorption in 35–300 °C over MCCX-Zn-Cl, MCCX-Zn-N, MCCX-Zn-S, and MCCX-Zn-C catalysts. Conditions: 500 ppm NH_3 and N_2 as balance.

Profiles of H_2-TPR for MCCX-Zn-Cl, MCCX-Zn-N, MCCX-Zn-S, and MCCX-Zn-C catalysts are shown in Figure 6. The MCCX-Zn-Cl catalyst was found to have three fitting peaks at 200–400 °C, but the other three Zn-poisoned catalysts only had two fitting peaks at 200–400 °C. For the peak at ca. 200 °C, CuO was reduced to Cu^0; for the peak at 250 °C, Cu^{2+} species on the hydroxyl group of zeolite X were reduced; and for the peak at 300 °C, isolated Cu^{2+} ions located in lattice zeolite X were reduced. The peak over 400 °C was related to the reduction of Cu^+ ions, and no peak existed in the Zn-poisoned catalysts. Peaks at ca. 200–500 °C belonged to the reductions of MnO_2 to Mn_2O_3, Mn_2O_3 to Mn_3O_4, and Mn_3O_4 to MnO. The CeO_2 redox process of surface-capping oxygen occurs at temperatures of ca. 400 °C [38–40]. In addition, the consumption of H_2 for the Zn-poisoned catalysts was as follows: MCCX-Zn-C (6.6 mmoL/g) > MCCX-Zn-S (6.2 mmoL/g) > MCCX-Zn-Cl (5.5 mmoL/g) > MCCX-Zn-N (2.7 mmoL/g). It was discovered that the reduction of MCCX catalysts was affected by the presence of various Zn species, particularly the isolated Cu^{2+} ions in lattice zeolite X and Cu^+ ions. It could be found that the Zn poisoning produced more copper oxides on MCCX-Zn-S and MCCX-Zn-C catalysts, and reduced the Cu^{2+} active sites.

2.5. In Situ DRIFTS Studies

2.5.1. NO + O_2 Reacting with Pre-Adsorbed NH_3 Species

In order to study the impact of various Zn species on surface acidity types of the catalysts, the in situ DRIFTS spectra of MCCX-Zn-Cl, MCCX-Zn-N, MCCX-Zn-S, and MCCX-Zn-C catalysts for NH_3 adsorption at 200 °C were investigated. As shown in Figure 7, the bands of Cu^{2+}-absorbing NH_3 species at 3182 and 3332 cm^{-1}, NH_4^+ species on Brønsted acid sites at 3272 cm^{-1} and 1390 cm^{-1}, and coordinated adsorbed NH_3 species on Lewis acid sites at 1610 cm^{-1} and 1260 cm^{-1} [9,35] gradually increased in intensity after NH_3 was introduced for 5 min. It could be found that the bands belonging to Lewis acid sites were much stronger than that of Brønsted acid sites on Zn-poisoned catalysts.

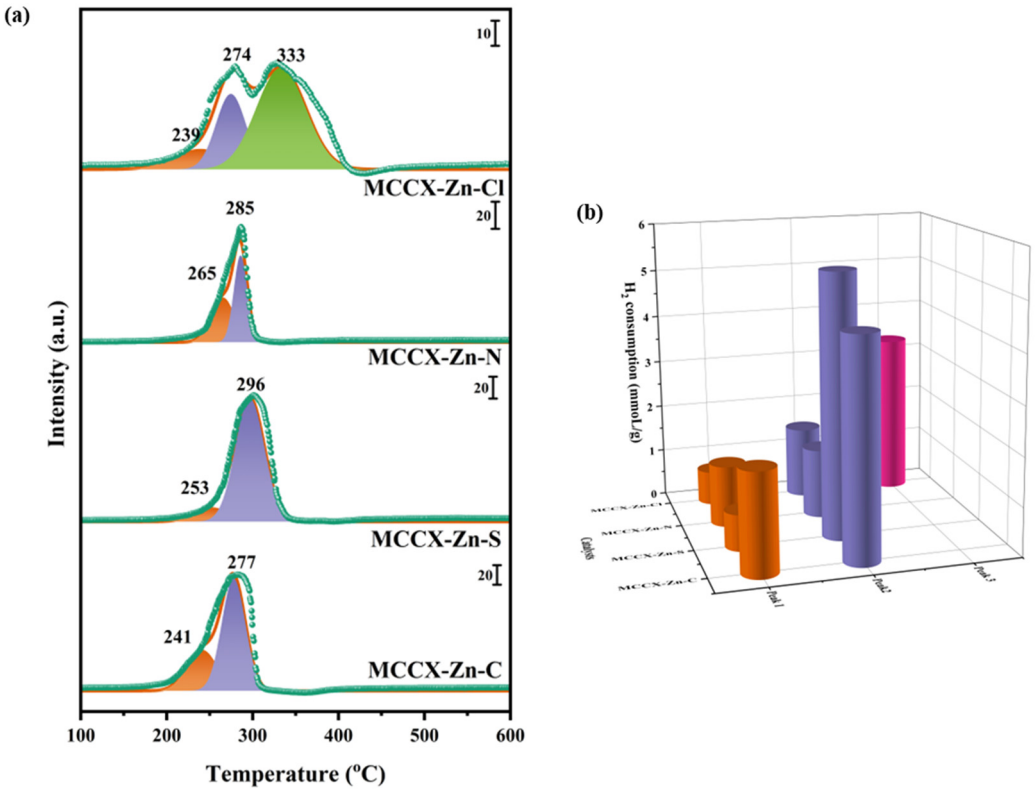

Figure 6. (**a**) H_2-TPR profiles of all catalyst (green solid dots were assigned to the original data, red line was assigned to the fitting curve, orange fitting peak related to peak 1, purple peak related to peak 2, green fitting peak related to peak 3) and (**b**) integral area of peaks from H_2-TPR profiles.

The intermediates of the reaction between NO + O_2 and pre-adsorbed NH_3 species at 200 °C were studied by performing in situ DRIFTS measurements over MCCX-Zn-Cl, MCCX-Zn-N, MCCX-Zn-S, and MCCX-Zn-C catalysts, as shown in Figure 8. When NH_3 was introduced, bands with intensities of Cu^{2+}-absorbing NH_3 species (3182 and 3332 cm^{-1}), NH_4^+ species on Brønsted acid sites (3272 cm^{-1} and 1390 cm^{-1}), and coordinated adsorbed NH_3 species on Lewis acid sites (1610 cm^{-1} and 1260 cm^{-1}) were observed on the four Zn-poisoned catalysts, and these bands disappeared after 20 min of NO + O_2 purging. After that, many striations, which could be attributed to various nitrate and nitrite species, began to show up. Nitrate species at the Cu^{2+} active site were attributed to the 1915 cm^{-1} band [41], while those at 1600–1650 cm^{-1} were characterized as bidentate bridging nitrate (M-O_2-NO), those at 1500–1570 cm^{-1} were described as bidentate chelating nitrate (M-O_2NO), those at 1480–1530 cm^{-1} as monodentate nitrate (M-O-NO_2), and those at 1317–1400 cm^{-1} as free-NO_3^- species of antisymmetric N-O stretches [35,42–44]. Bidentate nitrite (M-O_2N) and bridging nitrite (M-O_2-N) contributed the bands at 1320 cm^{-1} and 1575 cm^{-1}, respectively [42,45]. It indicated that both the Langmuir–Hinshelwood (L–H) and Eley–Rideal (E–R) mechanisms were at play in all of the catalysts. $ZnCl_2$ species on MCCX catalysts had a slight influence on the Cu^{2+} active site, while the band intensity of nitrate species on the Cu^{2+} active site for MCCX-Zn-S was weaker than that of the other three catalysts.

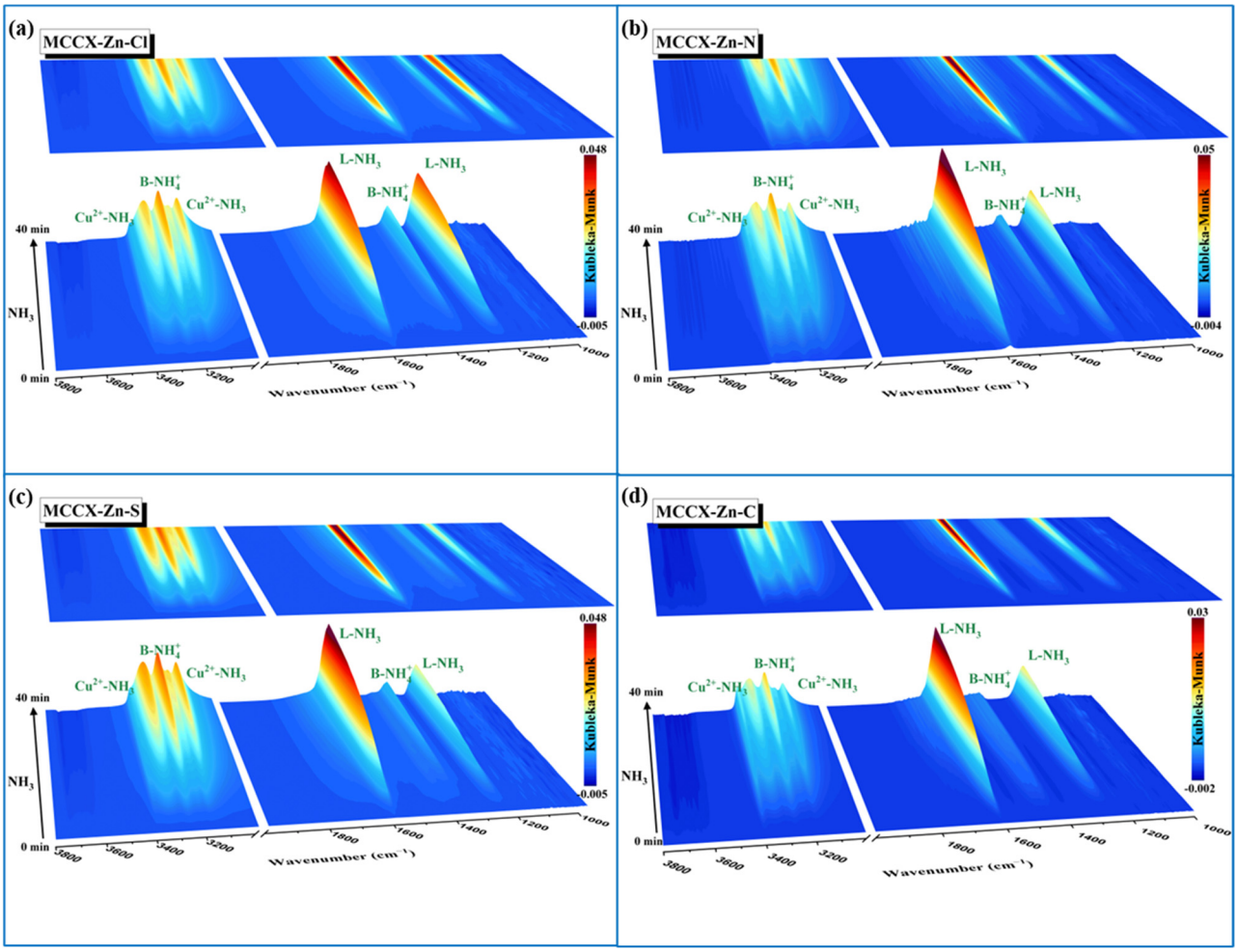

Figure 7. In situ DRIFTS spectra of (**a**) MCCX-Zn-Cl, (**b**) MCCX-Zn-N, (**c**) MCCX-Zn-S, and (**d**) MCCX-Zn-C catalysts for NH_3 adsorption at 200 °C. Conditions: 500 ppm NH_3 and N_2 as balance.

2.5.2. NH_3 Reacting with Pre-Adsorbed NO + O_2 Species

Figure 9 displays the in situ DRIFTS spectra of NO + O_2 co-adsorption at 200 °C over MCCX-Zn-Cl, MCCX-Zn-N, MCCX-Zn-S, and MCCX-Zn-C catalysts. The bands of bidentate bridging nitrate (M-O_2-NO) (at 1600–1650 cm^{-1}), bidentate chelating nitrate (M-O_2NO) (at 1500–1570 cm^{-1}), monodentate nitrate (M-O-NO_2) (at 1480–1530 cm^{-1}), and the free-NO_3^- species (at 1300–1400 cm^{-1}) of antisymmetric N-O stretches appeared, and the bands of nitrate species on Cu^{2+} active site (at 1915 cm^{-1}) appeared over the MCCX-Zn-Cl, MCCX-Zn-N, MCCX-Zn-S, and MCCX-Zn-C catalysts [35,42–45]. The longer they were exposed to NO + O_2, the stronger their bands became. It was found that the nitrate species adsorbing on the Cu^{2+} active site over the MCCX-Zn-Cl, MCCX-Zn-N, MCCX-Zn-S, and MCCX-Zn-C catalysts had much stronger band intensity than the other bands of nitrites and nitrates, suggesting that the Cu^{2+} active site was the primary site involved in the NO + O_2 adsorption. Further, the nitrate and nitrite intermediate products were significantly affected by the poisoning impact of $ZnCl_2$, $Zn(NO_3)_2$, and $ZnSO_4$ on MCCX catalysts, as compared to $ZnCO_3$.

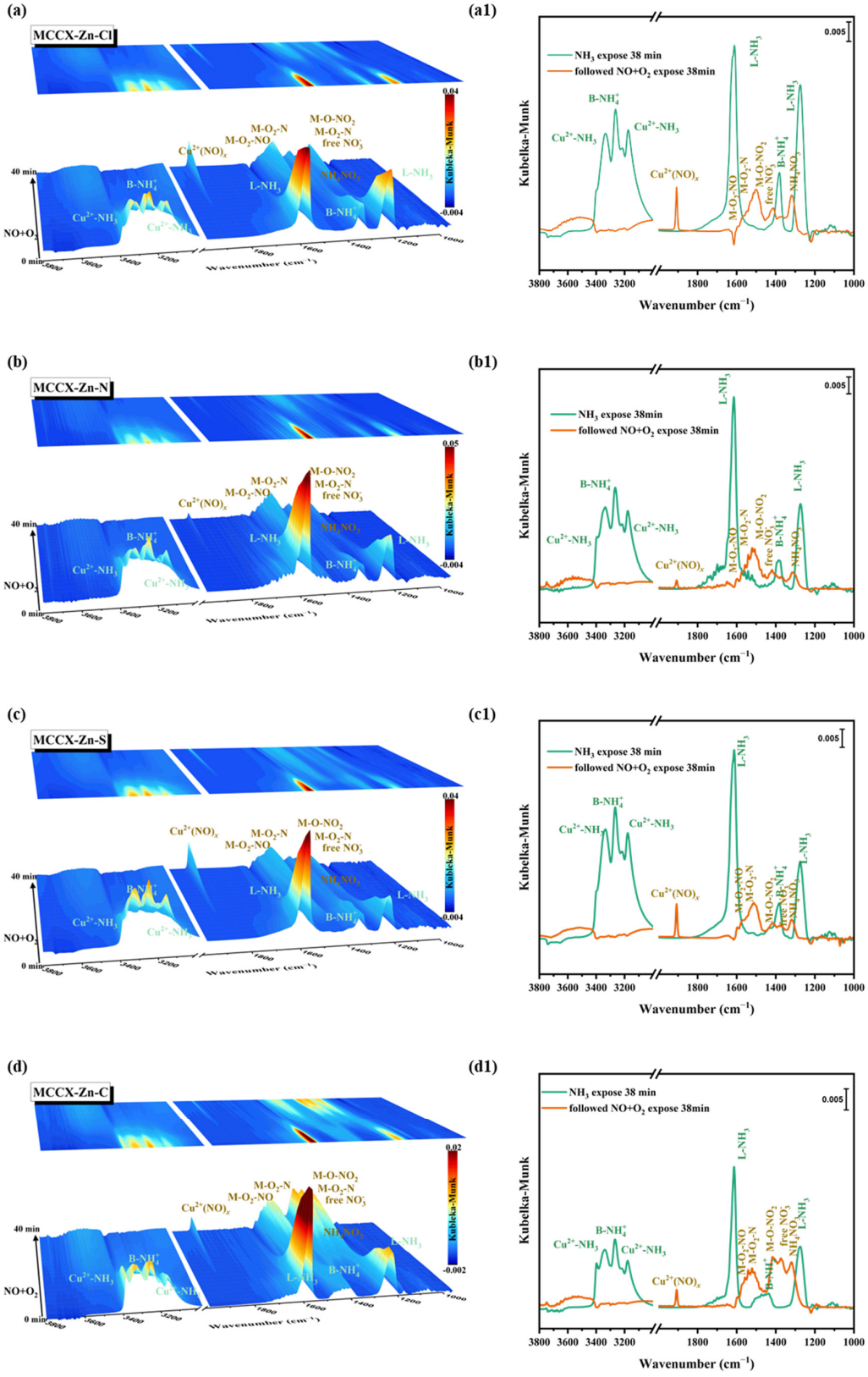

Figure 8. In situ DRIFTS spectra of (**a**) MCCX-Zn-Cl, (**b**) MCCX-Zn-N, (**c**) MCCX-Zn-S, and (**d**) MCCX-Zn-C catalysts for NO + O_2 reacting with pre-adsorbed NH_3 species at 200 °C; in situ DRIFTS spectra of (**a1**) MCCX-Zn-Cl, (**b1**) MCCX-Zn-N, (**c1**) MCCX-Zn-S, and (**d1**) MCCX-Zn-C catalysts for NH_3 adsorbed for 38 min and followed by NO + O_2 adsorbed for 38 min at 200 °C. Conditions: 500 ppm NH_3, 500 ppm NO, 11% O_2, and N_2 as balance.

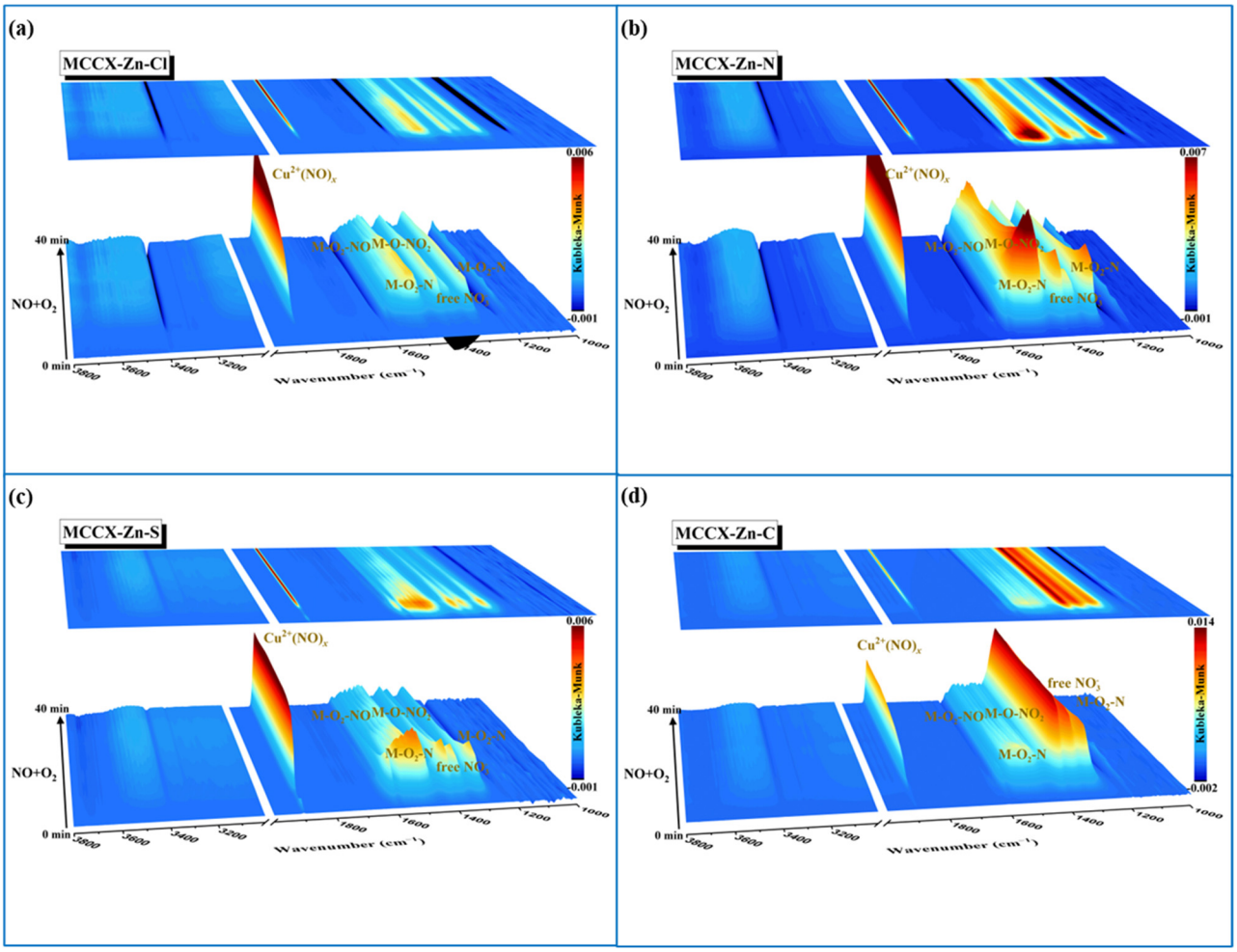

Figure 9. In situ DRIFTS spectra of (**a**) MCCX-Zn-Cl, (**b**) MCCX-Zn-N, (**c**) MCCX-Zn-S, and (**d**) MCCX-Zn-C catalysts for NO + O_2 co-adsorption at 200 °C. Conditions: 500 ppm NO, 11% O_2 and N_2 as balance.

Figure 10 displays the in situ DRIFTS measurements performed over the MCCX-Zn-Cl, MCCX-Zn-N, MCCX-Zn-S, and MCCX-Zn-C catalysts at 200 °C to investigate the reaction intermediates between NH_3 and pre-adsorbed NO + O_2 species. Nitrate species on the Cu^{2+} active site ($Cu(NO_3)_x$), bidentate bridging nitrate (M-O_2-NO), bidentate chelating nitrate (M-O_2NO), monodentate nitrate (M-O-NO_2), NH_4NO_3 species, and the free-NO_3^- species of antisymmetric N-O stretches all showed gradual decreasing trends in band intensity when NH_3 was introduced, which eventually disappeared after 15 min. Then, bands appeared at increasing intensities with increasing time of NH_3 exposure, which were attributed to Cu^{2+}-absorbing NH_3 species (3182 and 3332 cm^{-1}), NH_4^+ species on Brønsted acid sites (3272 cm^{-1}), and coordinated adsorbed NH_3 species on Lewis acid sites (1610 cm^{-1} and 1260 cm^{-1}).

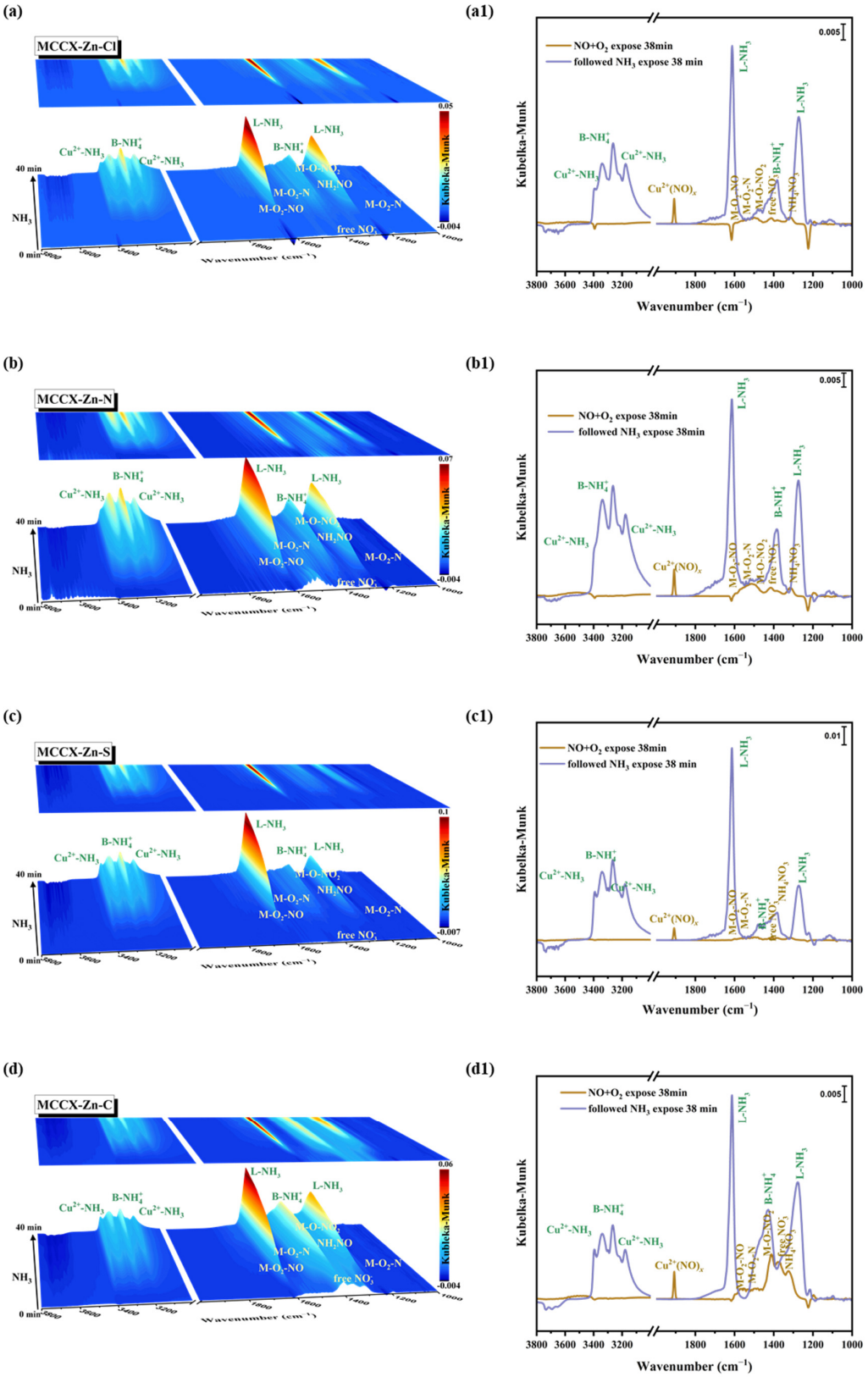

Figure 10. In situ DRIFTS spectra of (**a**) MCCX-Zn-Cl, (**b**) MCCX-Zn-N, (**c**) MCCX-Zn-S, and (**d**) MCCX-Zn-C catalysts for NH_3 reacting with pre-adsorbed NO + O_2 species at 200 °C; in situ DRIFTS spectra of (**a1**) MCCX-Zn-Cl, (**b1**) MCCX-Zn-N, (**c1**) MCCX-Zn-S, and (**d1**) MCCX-Zn-C catalysts for NO + O_2 adsorbed for 38 min and followed by NH_3 adsorbed for 38 min at 200 °C. Conditions: 500 ppm NH_3, 500 ppm NO, 11% O_2, and N_2 as balance.

3. Discussion

From the XRD results, it could be found that the zeolite X structure was impacted by Zn species doping on the MCCX catalyst, and the zinc species contributed to the migration of CuO species on the Zn-poisoned catalysts. Some of the zeolite X particles agglomerated, and Cu species aggregated on catalysts due to Zn poisoning, leading to insufficient Cu active sites from the SEM and EDS results. Furthermore, the zeolite X structure for the MCCX-Zn-S and MCCX-Zn-C catalysts had more serious damage. From the XPS analysis, it could be found that the MCCX-Zn-C catalyst had less Cu^{2+} species, while the MCCX-Zn-S catalyst had less Mn^{4+} species. The Cu^{2+} species and Mn^{4+} species were the main active sites for low-temperature SCR reaction, which might be the reason that the $ZnSO_4$ and $ZnCO_3$ on the MCCX catalyst had a more serious effect on catalytic activity. The MCCX-Zn-Cl catalyst had the strongest surface acidity, while the MCCX-Zn-S catalyst had the weakest surface acidity, which affected the adsorption of NH_3. From the H_2-TPR analysis, it could be found that Zn poisoning produced more copper oxides for MCCX-Zn-S and MCCX-Zn-C catalysts and reduced the Cu^{2+} active sites, thereby having an influence on NO and NH_3 adsorption. The bands belonging to Lewis acid sites were much stronger than that of Brønsted acid sites on Zn-poisoned catalysts from the in situ DRIFTS spectra of NH_3 adsorption. Based on the in situ DRIFTS spectra of NO + O_2 and NH_3 species, both the Langmuir–Hinshelwood (L–H) and Eley–Rideal (E–R) mechanisms were at play in all of the catalysts. $ZnCl_2$ species on MCCX catalysts had a slight influence on the Cu^{2+} active site, while the band intensity of nitrate species on the Cu^{2+} active site for MCCX-Zn-S was weaker than that of the other three catalysts. The scheme of mechanism effect for different zinc species on the Mn-Ce/CuX catalyst is summarized in Figure 11.

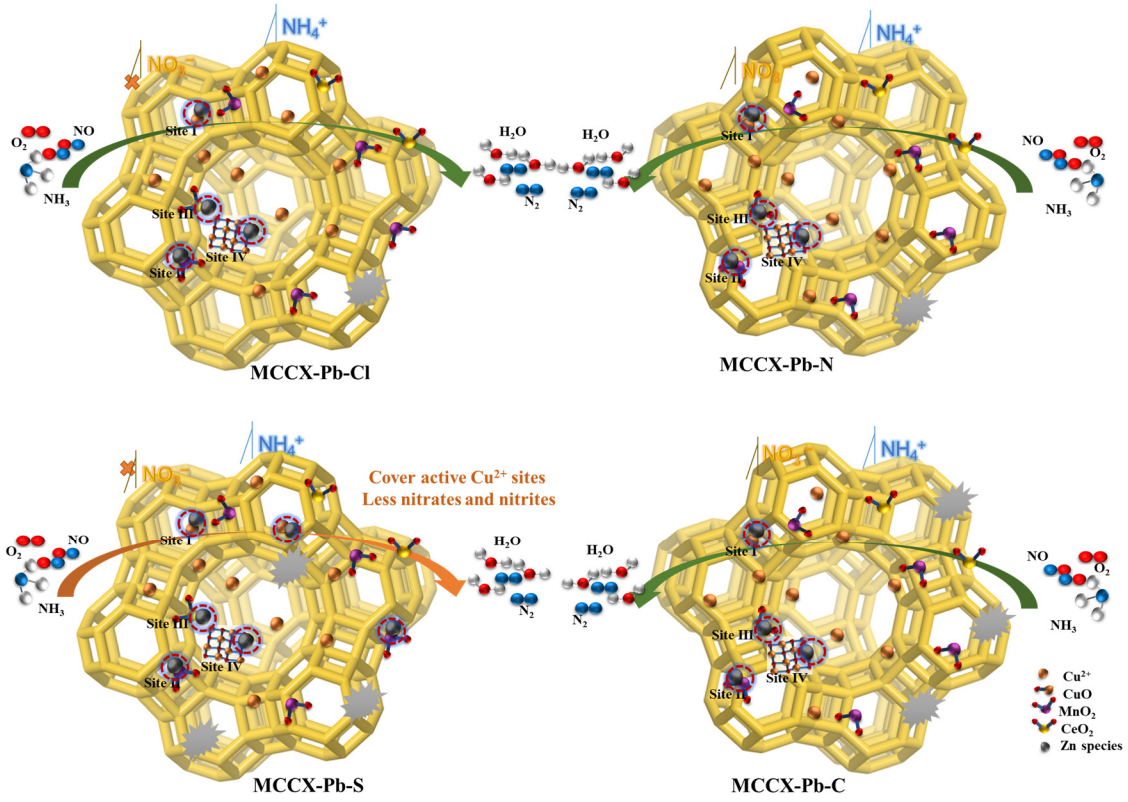

Figure 11. Scheme of mechanism effect for different zinc species on Mn-Ce/CuX catalyst.

4. Materials and Methods

4.1. Catalysts Preparation

The Mn-Ce/CuX catalysts utilized in this study were synthesized using the impregnation method, with the Mn-Ce mixed oxides loading of 5 wt.% (molar ratio of Mn/Ce was

7:3), and the details of the preparation process were described in our earlier study [19]. The first synthesis of CuX catalyst included both hydrothermal and ion exchange methods [13]. After obtaining CuX catalysts, they were added into a precursor solution including a predetermined amount of manganous nitrate and cerous nitrate, and the resulting slurry was dried out in a water bath at 80 °C. The Mn-Ce/CuX catalyst was produced by drying in an oven for 10 h at 80 °C and then calcining them in a muffle furnace for 3 h at 500 °C in air condition.

A total of 1 wt.% Zn species was used to poison the Mn-Ce/CuX catalysts, which were then composited using an impregnation approach in a variety of zinc compounds which were $ZnCl_2$, $Zn(NO_3)_2$, $ZnSO_4$, and $ZnCO_3$, respectively. After evaporating the solutions of $ZnCl_2$, $Zn(NO_3)_2$, $ZnSO_4$, and $ZnCO_3$ in an 80 °C water bath, the samples were dried in an 80 °C oven and then calcinated for 3 h at 500 °C in air. MCCX-Zn-Cl, MCCX-Zn-N, MCCX-Zn-S, and MCCX-Zn-C were the names assigned to the several Zn-poisoned catalysts for $ZnCl_2$, $Zn(NO_3)_2$, $ZnSO_4$, and $ZnCO_3$.

4.2. Catalytic Activity Tests

The NH_3-SCR activity of the MCCX-Zn-Cl, MCCX-Zn-N, MCCX-Zn-S, and MCCX-Zn-C catalysts was studied in a 10 mm diameter quartz reactor using 0.5 g (40–60 mesh) samples. The temperature went from 75 to 300 °C in increments of 25 °C, and each temperature point was maintained for 30 min. The simulant mixed gas contained 500 ppm NH_3, 500 ppm NO, 11 vol% O_2, and N_2 as balanced gas with a total flow gas of 100 mL/min and an hourly space velocity of 36,000 h^{-1}. The amount of NO, NH_3, NO_2, and N_2O coming out was measured by a gas analyzer (Thermo Scientific, Antaris IGS, Waltham, MA, USA). The NO conversion and N_2 selectivity of the MCCX-Zn-Cl, MCCX-Zn-N, MCCX-Zn-S, and MCCX-Zn-C catalysts were determined using the following equations (Equations (1) and (2)) [27,37].

$$\text{NO conversion } (\%) = \left(1 - \frac{[NO]_{out}}{[NO]_{in}}\right) \times 100\% \quad (1)$$

$$N_2 \text{ selectivity } (\%) = \left(1 - \frac{2[N_2O]_{out} - [NO_2]_{out}}{[NO]_{in} + [NH_3]_{in} - [NO]_{out} - [NH_3]_{out}}\right) \times 100\% \quad (2)$$

4.3. Catalyst Characterization

The X-ray diffraction (XRD) patterns were conducted to examine the composition and crystallinity of chemicals on the catalyst surface using the Rigaku D/max-2500 PC diffractometer which was recorded with a 2θ range of 5–90° at a scanning speed of 5°/min. Scanning electron microscope (SEM) analysis was used to investigate the surface microstructure of MCCX-Zn-Cl, MCCX-Zn-N, MCCX-Zn-S, and MCCX-Zn-C catalysts by the Thermo Scientific Quattro SEM. The content and distribution of surface elements were recorded using energy dispersive X-ray spectrometry (EDS) mapping.

X-ray photoelectron spectroscopy (XPS) experiments were used to measure the Cu 2p, O 1s, Mn 2p, and Zn 2p by the Thermo ESCALAB 250Xi with Al Kα radiation (1484.6 eV) at room temperature. The binding energy of the surface elements of the sample was calibrated using C 1s (284.6 eV), and the sample was degassed in a vacuum for 1 h before testing to minimize the influence of surface impurities.

A H_2-TPR test was used on an Auto Chem II TPR/TPD 2920 detector. The specific operation process was as follows: 150 mg of catalyst was placed in the U-shaped quartz reaction tube, and the sample was pretreated under Ar flow of 100 mL/min. Then, the sample was heated from room temperature to 300 °C at a heating rate of 5 °C/min and then cooled to 50 °C after purging for 1 h, after which the sample was heated to 600 °C (heating rate of 10 °C/min) under 5% H_2/Ar atmosphere (flow rate of 50 mL/min). At the same time, the detector recorded the TCD signal. NH_3-TPD tests were conducted by the Chembet Pulsar TPR/TPD detector (The American Konta Company), and the pretreated

steps were the same as H_2-TPR. The sample was then exposed to a 5% NH_3/Ar atmosphere (flow rate of 100 mL/min) for 1 h and followed by purging in N_2 (100 mL/min). Then, the sample was heated to 800 °C at a constant heating rate of 5 °C/min under a flow of 100 mL/min Ar, and the TCD signal was detected.

In situ diffuse reflectance infrared Fourier transform (in situ DRIFTS) studies were investigated on the Thermo Fisher Nicolet iS50 spectrometer. Before the test, all the catalysts were purged at 300 °C for 30 min under N_2 and 11 vol% O_2 atmosphere (total flow rate of 100 mL/min); then, the background spectrum at a desired temperature was collected. Then, the catalysts were exposed under 500 ppm NH_3/N_2 or 500 ppm NO/N_2 and 11 vol% O_2 gas for 40 min (total flow rate of 100 mL/min), after which they were flushed under N_2 gas for 60 min.

5. Conclusions

This research investigated and contrasted the effects of four distinct zinc species ($ZnCl_2$, $Zn(NO_3)_2$, $ZnSO_4$, and $ZnCO_3$) on the Mn-Ce co-doped CuX catalyst in a low-temperature NH_3-SCR process. Poisoned catalysts were made by impregnating in aqueous solutions of zinc chloride, zinc nitrate, zinc sulfate, and zinc carbonate. All catalysts' NH_3-SCR activity were quantified, and the physicochemical characteristics were studied. There was a notable drop in catalytic activity for the catalyst in the low temperature range after zinc species poisoning, with the order of poisoning going as follows: $ZnSO_4 > ZnCO_3 > Zn(NO_3)_2 > ZnCl_2$. Zn species affected the reduction of the MCCX catalyst, especially isolated Cu^{2+} ions in lattice zeolite X, leading to a decrease in the SCR activity. $ZnSO_4$'s poisoning effect on MCCX catalysts was much more pronounced on the nitrate and nitrite intermediate products than that of $ZnCO_3$, $ZnCl_2$, and $Zn(NO_3)_2$, and all the catalysts were governed by both the Langmuir–Hinshelwood (L–H) and Eley–Rideal (E–R) mechanism as evidenced by the in situ DRIFTS spectra.

Author Contributions: L.C.: conceptualization, methodology, writing—original draft, investigation, formal analysis. S.R.: conceptualization, supervision, methodology, resources, funding acquisition, writing—review and editing, resources. T.C.: investigation, formal analysis. X.L.: investigation, formal analysis. Z.C.: investigation, visualization. M.W.: validation, writing—review and editing. Q.L.: conceptualization, project administration. J.Y.: investigation, formal analysis. All authors have read and agreed to the published version of the manuscript.

Funding: This research was funded by the National Natural Science Foundation of China, grant No. 52174298, and Shanxi Provincial Innovation Capacity Support Plan, grant number No. 2023-CX-TD-53.

Data Availability Statement: We are happy to share our research data.

Conflicts of Interest: The authors declare no conflict of interest.

References

1. Anenberg, S.C.; Miller, J.; Minjares, R.; Du, L.; Henze, D.K.; Lacey, F.; Malley, C.S.; Emberson, L.; Franco, V.; Klimont, Z.; et al. Impacts and mitigation of excess diesel-related NO_x emissions in 11 major vehicle markets. *Nature* **2017**, *545*, 467–471. [CrossRef]
2. Wuebbles, D.J. Atmosphere. Nitrous oxide: No laughing matter. *Science* **2009**, *326*, 56–57. [CrossRef] [PubMed]
3. Peng, H.; Dong, T.; Yang, S.; Chen, H.; Yang, Z.; Liu, W.; He, C.; Wu, P.; Tian, J.; Peng, Y.; et al. Intra-crystalline mesoporous zeolite encapsulation-derived thermally robust metal nanocatalyst in deep oxidation of light alkanes. *Nat. Commun.* **2022**, *13*, 295. [CrossRef] [PubMed]
4. Inomata, Y.; Kubota, H.; Hata, S.; Kiyonaga, E.; Morita, K.; Yoshida, K.; Sakaguchi, N.; Toyao, T.; Shimizu, K.I.; Ishikawa, S.; et al. Bulk tungsten-substituted vanadium oxide for low-temperature NO_x removal in the presence of water. *Nat. Commun.* **2021**, *12*, 557. [CrossRef] [PubMed]
5. Song, I.; Lee, H.; Jeon, S.W.; Ibrahim, I.A.M.; Kim, J.; Byun, Y.; Koh, D.J.; Han, J.W.; Kim, D.H. Simple physical mixing of zeolite prevents sulfur deactivation of vanadia catalysts for NO_x removal. *Nat. Commun.* **2021**, *12*, 901. [CrossRef]
6. Guo, Y.; Xu, X.; Gao, H.; Zheng, Y.; Luo, L.; Zhu, T. Ca-poisoning effect on V_2O_5-WO_3/TiO_2 and V_2O_5-WO_3-CeO_2/TiO_2 catalysts with different vanadium loading. *Catalysts* **2021**, *11*, 445. [CrossRef]
7. Negri, C.; Selleri, T.; Borfecchia, E.; Martini, A.; Lomachenko, K.A.; Janssens, T.V.W.; Cutini, M.; Bordiga, S.; Berlier, G. Structure and reactivity of oxygen-bridged diamino dicopper(II) complexes in Cu-ion-exchanged Chabazite catalyst for NH_3-mediated selective catalytic reduction. *J. Am. Chem. Soc.* **2020**, *142*, 15884–15896. [CrossRef]

8. Hu, W.; Gramigni, F.; Nasello, N.D.; Usberti, N.; Iacobone, U.; Liu, S.; Nova, I.; Gao, X.; Tronconi, E. Dynamic binuclear CuII sites in the reduction half-cycle of low-temperature NH_3–SCR over Cu-CHA catalysts. *ACS Catal.* **2022**, *12*, 5263–5274. [CrossRef]
9. Wang, H.; Jia, J.; Liu, S.; Chen, H.; Wei, Y.; Wang, Z.; Zheng, L.; Wang, Z.; Zhang, R. Highly efficient NO abatement over Cu-ZSM-5 with special nanosheet features. *Environ. Sci. Technol.* **2021**, *55*, 5422–5434. [CrossRef]
10. Hu, W.; Iacobone, U.; Gramigni, F.; Zhang, Y.; Wang, X.; Liu, S.; Zheng, C.; Nova, I.; Gao, X.; Tronconi, E. Unraveling the hydrolysis of Z_2Cu^{2+} to $ZCu^{2+}(OH)^-$ and its consequences for the low-temperature selective catalytic reduction of NO on Cu-CHA catalysts. *ACS Catal.* **2021**, *11*, 11616–11625. [CrossRef]
11. Abdul Nasir, J.; Guan, J.; Keal, T.W.; Desmoutier, A.W.; Lu, Y.; Beale, A.M.; Catlow, C.R.A.; Sokol, A.A. Influence of solvent on selective catalytic reduction of nitrogen oxides with ammonia over Cu-CHA zeolite. *J. Am. Chem. Soc.* **2023**, *145*, 247–259. [CrossRef] [PubMed]
12. Tarach, K.A.; Jabłońska, M.; Pyra, K.; Liebau, M.; Reiprich, B.; Gläser, R.; Góra-Marek, K. Effect of zeolite topology on NH_3-SCR activity and stability of Cu-exchanged zeolites. *Appl. Catal. B* **2021**, *284*, 119752. [CrossRef]
13. Chen, L.; Ren, S.; Xing, X.; Yang, J.; Yang, J.; Wang, M.; Chen, Z.; Liu, Q. Low-cost CuX catalyst from blast furnace slag waste for low-temperature NH_3-SCR: Nature of Cu active sites and influence of SO_2/H_2O. *ACS Sustain. Chem. Eng.* **2022**, *10*, 7739–7751. [CrossRef]
14. Chen, L.; Ren, S.; Jiang, Y.; Liu, L.; Wang, M.; Yang, J.; Chen, Z.; Liu, W.; Liu, Q. Effect of Mn and Ce oxides on low-temperature NH_3-SCR performance over blast furnace slag-derived zeolite X supported catalysts. *Fuel* **2022**, *320*, 123969. [CrossRef]
15. Wang, X.; Liu, Y.; Wu, Z. The poisoning mechanisms of different zinc species on a ceria-based NH_3-SCR catalyst and the co-effects of zinc and gas-phase sulfur/chlorine species. *J. Colloid Interface Sci.* **2020**, *566*, 153–162. [CrossRef]
16. Su, Z.; Ren, S.; Yang, J.; Yao, L.; Zhou, Y.; Chen, Z.; Zhang, T. Poisoning effect comparison of $ZnCl_2$ and $ZnSO_4$ on Mn-Ce/AC catalyst for low-temperature SCR of NO. *ChemistrySelect* **2020**, *5*, 9226–9234. [CrossRef]
17. Zhou, Y.; Su, B.; Ren, S.; Chen, Z.; Su, Z.; Yang, J.; Chen, L.; Wang, M. Nb_2O_5-modified Mn-Ce/AC catalyst with high $ZnCl_2$ and SO_2 tolerance for low-temperature NH_3-SCR of NO. *J. Environ. Chem. Eng.* **2021**, *9*, 106323. [CrossRef]
18. Chen, L.; Ren, S.; Peng, H.; Yang, J.; Wang, M.; Chen, Z.; Liu, Q. Low-cost Mn-Ce/CuX catalyst from blast furnace slag waste for efficient low-temperature NH_3-SCR. *Appl. Catal. A-Gen.* **2022**, *646*, 118868. [CrossRef]
19. Usberti, N.; Gramigni, F.; Nasello, N.D.; Iacobone, U.; Selleri, T.; Hu, W.; Liu, S.; Gao, X.; Nova, I.; Tronconi, E. An experimental and modelling study of the reactivity of adsorbed NH_3 in the low temperature NH_3-SCR reduction half-cycle over a Cu-CHA catalyst. *Appl. Catal. B* **2020**, *279*, 119397. [CrossRef]
20. Guo, A.; Xie, K.; Lei, H.; Rizzotto, V.; Chen, L.; Fu, M.; Chen, P.; Peng, Y.; Ye, D.; Simon, U. Inhibition effect of phosphorus poisoning on the dynamics and redox of Cu active sites in a Cu-SSZ-13 NH_3-SCR catalyst for NO_x reduction. *Environ. Sci. Technol.* **2021**, *55*, 12619–12629. [CrossRef]
21. Chen, P.; Rauch, D.; Weide, P.; Schönebaum, S.; Simons, T.; Muhler, M.; Moos, R.; Simon, U. The effect of Cu and Fe cations on NH_3-supported proton transport in $DeNO_x$-SCR zeolite catalysts. *Catal. Sci. Technol.* **2016**, *6*, 3362–3366. [CrossRef]
22. Li, G.; Mao, D.; Chao, M.; Li, G.; Yu, J.; Guo, X. Significantly enhanced Pb resistance of a Co-modified Mn–Ce–O_x/TiO_2 catalyst for low-temperature NH_3-SCR of NO_x. *Catal. Sci. Technol.* **2020**, *10*, 6368–6377. [CrossRef]
23. Chen, L.; Ren, S.; Xing, X.; Yang, J.; Li, X.; Wang, M.; Chen, Z.; Liu, Q. Poisoning mechanism of KCl, K_2O and SO_2 on Mn-Ce/CuX catalyst for low-temperature SCR of NO with NH_3. *Process Saf. Environ. Prot.* **2022**, *167*, 609–619. [CrossRef]
24. Fang, X.; Liu, Y.; Cheng, Y.; Cen, W. Mechanism of Ce-modified birnessite-MnO_2 in promoting SO_2 poisoning resistance for low-temperature NH_3-SCR. *ACS Catal.* **2021**, *11*, 4125–4135. [CrossRef]
25. Yang, W.; Su, Z.a.; Xu, Z.; Yang, W.; Peng, Y.; Li, J. Comparative study of α-, β-, γ- and δ-MnO_2 on toluene oxidation: Oxygen vacancies and reaction intermediates. *Appl. Catal. B* **2020**, *260*, 118150. [CrossRef]
26. Fan, H.; Fan, J.; Chang, T.; Wang, X.; Wang, X.; Huang, Y.; Zhang, Y.; Shen, Z. Low-temperature Fe–MnO_2 nanotube catalysts for the selective catalytic reduction of NO_x with NH_3. *Catal. Sci. Technol.* **2021**, *11*, 6553–6563. [CrossRef]
27. Yan, R.; Lin, S.; Li, Y.; Liu, W.; Mi, Y.; Tang, C.; Wang, L.; Wu, P.; Peng, H. Novel shielding and synergy effects of Mn-Ce oxides confined in mesoporous zeolite for low temperature selective catalytic reduction of NO_x with enhanced SO_2/H_2O tolerance. *J. Hazard. Mater.* **2020**, *396*, 122592. [CrossRef]
28. Chen, J.; Zhao, R.; Zhou, R. A new insight into active Cu^{2+} species properties in one-pot synthesized Cu-SSZ-13 catalysts for NO_x reduction by NH_3. *ChemCatChem* **2018**, *10*, 5182–5189. [CrossRef]
29. Chen, B.; Xu, R.; Zhang, R.; Liu, N. Economical way to synthesize SSZ-13 with abundant ion-exchanged Cu^+ for an extraordinary performance in selective catalytic reduction (SCR) of NO_x by ammonia. *Environ. Sci. Technol.* **2014**, *48*, 13909–13916. [CrossRef]
30. Yao, X.; Zhang, L.; Li, L.; Liu, L.; Cao, Y.; Dong, X.; Gao, F.; Deng, Y.; Tang, C.; Chen, Z. Investigation of the structure, acidity, and catalytic performance of $CuO/Ti_{0.95}Ce_{0.05}O_2$ catalyst for the selective catalytic reduction of NO by NH_3 at low temperature. *Appl. Catal. B* **2014**, *150–151*, 315–329. [CrossRef]
31. Kang, K.; Yao, X.; Huang, Y.; Cao, J.; Rong, J.; Zhao, W.; Luo, W.; Chen, Y. Insights into the co-doping effect of Fe^{3+} and Zr^{4+} on the anti-K performance of $CeTiO_x$ catalyst for NH_3-SCR reaction. *J. Hazard. Mater.* **2021**, *416*, 125821. [CrossRef] [PubMed]
32. Wei, L.; Wang, Z.; Liu, Y.; Guo, G.; Dai, H.; Cui, S.; Deng, J. Support promotion effect on the SO_2 and K^+ co-poisoning resistance of MnO_2/TiO_2 for NH_3-SCR of NO. *J. Hazard. Mater.* **2021**, *416*, 126117. [CrossRef]
33. Yu, Y.; Geng, M.; Li, J.; Wang, J.; Wei, D.; He, C. The different effect of SO_2 on Zn-poisoned commercial V_2O_5-WO_3/TiO_2 catalysts with varied Zn loading. *Chem. Phys. Impact* **2023**, *6*, 100150. [CrossRef]

34. Xue, H.; Guo, X.; Meng, T.; Mao, D.; Ma, Z. Poisoning effect of K with respect to Cu/ZSM-5 used for NO reduction. *Colloid Interface Sci. Commun.* **2021**, *44*, 100465. [CrossRef]
35. Negri, C.; Hammershoi, P.S.; Janssens, T.V.W.; Beato, P.; Berlier, G.; Bordiga, S. Investigating the low temperature formation of Cu(II)-(N,O) species on Cu-CHA zeolites for the selective catalytic reduction of NO_x. *Chemistry* **2018**, *24*, 12044–12053. [CrossRef] [PubMed]
36. Wang, Z.; Guo, R.; Shi, X.; Liu, X.; Qin, H.; Liu, Y.; Duan, C.; Guo, D.; Pan, W. The superior performance of $CoMnO_x$ catalyst with ball-flowerlike structure for low-temperature selective catalytic reduction of NO_x by NH_3. *Chem. Eng. J.* **2020**, *381*, 122753. [CrossRef]
37. Zhang, Y.; Zhu, H.; Zhang, T.; Li, J.; Chen, J.; Peng, Y.; Li, J. Revealing the synergistic deactivation mechanism of hydrothermal aging and SO_2 poisoning on Cu/SSZ-13 under SCR condition. *Environ. Sci. Technol.* **2022**, *56*, 1917–1926. [CrossRef]
38. Wang, X.; Liu, Y.; Wu, Z. Highly active $NbOPO_4$ supported Cu-Ce catalyst for NH_3-SCR reaction with superior sulfur resistance. *Chem. Eng. J.* **2020**, *382*, 122941. [CrossRef]
39. Stanciulescu, M.; Bulsink, P.; Caravaggio, G.; Nossova, L.; Burich, R. NH_3-TPD-MS study of Ce effect on the surface of Mn- or Fe-exchanged zeolites for selective catalytic reduction of NO_x by ammonia. *Appl. Surf. Sci.* **2014**, *300*, 201–207. [CrossRef]
40. Zhou, X.; Huang, X.; Xie, A.; Luo, S.; Yao, C.; Li, X.; Zuo, S. V_2O_5-decorated Mn-Fe/attapulgite catalyst with high SO_2 tolerance for SCR of NO_x with NH_3 at low temperature. *Chem. Eng. J.* **2017**, *326*, 1074–1085. [CrossRef]
41. Li, Y.; Deng, J.; Song, W.; Liu, J.; Zhao, Z.; Gao, M.; Wei, Y.; Zhao, L. Nature of Cu species in Cu–SAPO-18 catalyst for NH_3–SCR: Combination of experiments and DFT calculations. *J. Phys. Chem. C* **2016**, *120*, 14669–14680. [CrossRef]
42. Yang, J.; Ren, S.; Zhou, Y.; Su, Z.; Yao, L.; Cao, J.; Jiang, L.; Hu, G.; Kong, M.; Yang, J.; et al. In situ IR comparative study on N_2O formation pathways over different valence states manganese oxides catalysts during NH_3–SCR of NO. *Chem. Eng. J.* **2020**, *397*, 125446. [CrossRef]
43. Li, Q.; Gu, H.C.; Li, P.; Zhou, Y.H.; Liu, Y.; Qi, Z.N.; Xin, Y.; Zhang, Z.L. In situ IR studies of selective catalytic reduction of NO with NH_3 on Ce-Ti amorphous oxides. *Chin. J. Catal.* **2014**, *35*, 1289. [CrossRef]
44. Yang, S.; Xiong, S.; Liao, Y.; Xiao, X.; Qi, F.; Peng, Y.; Fu, Y.; Shan, W.; Li, J. Mechanism of N2O formation during the low-temperature selective catalytic reduction of NO with NH_3 over Mn-Fe spinel. *Environ. Sci. Technol.* **2014**, *48*, 10354–10362. [CrossRef] [PubMed]
45. Yao, L.; Liu, Q.; Mossin, S.; Nielsen, D.; Kong, M.; Jiang, L.; Yang, J.; Ren, S.; Wen, J. Promotional effects of nitrogen doping on catalytic performance over manganese-containing semi-coke catalysts for the NH_3-SCR at low temperatures. *J. Hazard. Mater.* **2020**, *387*, 121704. [CrossRef] [PubMed]